Stem Cell Reports
Article

ISSCR

OPEN ACCESS

Functional and Pharmacological Analysis of Cardiomyocytes Differentiated from Human Peripheral Blood Mononuclear-Derived Pluripotent Stem Cells

Michael Riedel,[1,4] Chuanchau J. Jou,[2,3,4] Shuping Lai,[1] Robert L. Lux,[3] Alonso P. Moreno,[3] Kenneth W. Spitzer,[3] Elizabeth Christians,[1] Martin Tristani-Firouzi,[2,3,*] and Ivor J. Benjamin[1,*]
[1]Cardiovascular Center, Medical College of Wisconsin, Milwaukee, WI 53226, USA
[2]Division of Pediatric Cardiology, University of Utah School of Medicine, Salt Lake City, UT 83113, USA
[3]Nora Eccles Harrison CVRTI, University of Utah School of Medicine, Salt Lake City, UT 84112, USA
[4]Co-first author
*Correspondence: mfirouzi@cvrti.utah.edu (M.T.-F.), ibenjamin@mcw.edu (I.J.B.)
http://dx.doi.org/10.1016/j.stemcr.2014.04.017

SUMMARY

Advances in induced pluripotent stem cell (iPSC) technology have set the stage for routine derivation of patient- and disease-specific human iPSC-cardiomyocyte (CM) models for preclinical drug screening and personalized medicine approaches. Peripheral blood mononuclear cells (PBMCs) are an advantageous source of somatic cells because they are easily obtained and readily amenable to transduction. Here, we report that the electrophysiological properties and pharmacological responses of PBMC-derived iPSC CM are generally similar to those of iPSC CM derived from other somatic cells, using patch-clamp, calcium transient, and multielectrode array (MEA) analyses. Distinct iPSC lines derived from a single patient display similar electrophysiological features and pharmacological responses. Finally, we demonstrate that human iPSC CMs undergo acute changes in calcium-handling properties and gene expression in response to rapid electrical stimulation, laying the foundation for an in-vitro-tachypacing model system for the study of human tachyarrhythmias.

INTRODUCTION

The reprogramming of somatic cells to induced pluripotent stem cells (iPSCs) has revolutionized the fields of biology and medicine, providing new avenues for research and regenerative medicine applications. IPSCs are typically generated from somatic cells by overexpression of a set of pluripotency-specific transcription factors (Takahashi et al., 2007; Takahashi and Yamanaka, 2006; Yu et al., 2007). For many years, the fibroblast has been the main source from which to derive human iPSCs (hIPSCs), and numerous publications have described the functional properties of cardiomyocytes (CMs) differentiated from fibroblast-derived iPSCs (Itzhaki et al., 2011, 2012; Lahti et al., 2012; Liang et al., 2013; Malan et al., 2011; Matsa et al., 2011; Moretti et al., 2010; Navarrete et al., 2013; Yazawa et al., 2011). Disadvantages of fibroblasts, however, as a somatic cell source include the need for a minor surgical procedure (skin biopsy) and the requirement for several weeks of expansion prior to reprogramming (Lowry et al., 2008). To overcome these hurdles, Staerk and colleagues developed an approach to generate hiPSCs from peripheral blood T and myeloid cells that allows for transduction shortly after harvesting (Staerk et al., 2010).

Here, we report the electrophysiological and pharmacological characterization of CMs differentiated from human peripheral blood mononuclear cell (PBMC)-derived iPSCs, using the patch-clamp technique, calcium transient (CaT) measurements, and multielectrode array (MEA) recordings. MEA-based assays using hiPSC-derived CMs are an attractive platform for the preclinical evaluation of potential QT-prolonging drug effects, a major obstacle in drug development, and the prevention of adverse outcomes. Most hiPSCCM studies report the field potential duration as a measure of repolarization, although this measure has no direct correlate to the transmembrane action potential duration (APD). The activation-recovery interval (ARI) is a direct correlate of APD and has been extensively validated in animal models and human studies (Chinushi et al., 2001; Fuller et al., 2000a; Haws and Lux, 1990; Yue et al., 2004). In this study, we report the ARI as a robust, spatiotemporal measure of repolarization particularly when applied to the effects of pharmacological treatment of hiPSC CM in culture. Such proof-of-principal experiments provide a platform to study the (patho)physiological interactions between the initiating factors and the substrates underlying human tachyarrhythmias and to test the in vitro efficacy of Food and Drug Administration-approved therapeutic interventions.

RESULTS

Derivation of hiPSC Lines and Proof of Pluripotency

PBMC transduction with lentiviral STEMCCA vectors generated multiple iPSC clones. Of ten iPSC clones generated, three were selected for subsequent characterization and differentiation into CMs (Figures 1 and 2). Transduced cells grew in typically shaped colonies and resembled

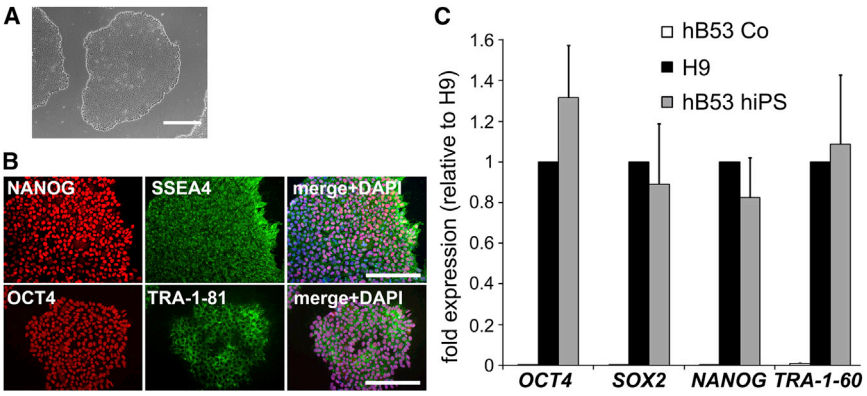

Figure 1. Characterization of Human Peripheral Blood Monocyte-Derived iPSCs

(A) Representative image of iPSC colonies in bright field. Scale bar, 200 μm.

(B) Representative images of iPSC colonies after immunostaining for the pluripotency markers NANOG, SSEA-4, OCT-4, and TRA-1-81. The merged images additionally include a DAPI staining for DNA to show that the transcription factors and pluripotency markers NANOG and OCT-4 are localized within the nuclei of the cells. Scale bars, 100 μm.

(C) Pluripotency gene expression levels as revealed by quantitative real-time PCR. Gene expression levels of undifferentiated hiPSCs (gray bars) are very similar to those of the undifferentiated human H9 cells (black bars). hB53 controls (Co) (uninfected blood mononuclear cells) show practically no pluripotency gene expression levels (white bars) (n = 3 independent experiments). Error bars, SD.

human embryonic stem cell (ESC) colonies (Figure 1A). Evaluation of metaphase cells from the colonies revealed a normal male chromosome karyotype. To establish the pluripotency of the generated hiPSC lines, we first analyzed the mRNA expression levels of the endogenous *OCT-4*, *SOX2*, *NANOG*, and *TRA-1-60* expression levels with RT-quantitative PCR (qPCR) (Figure 1C). Expression of the tested genes was significantly higher in hB53 iPSCs compared with parental PBMCs. Moreover, the gene expression levels of iPSCs were similar to the human ESC line H9. Accordingly, immunocytochemistry staining of hiPSCs revealed that human stem cell marker proteins such as NANOG, SSEA4, OCT4, and TRA-1-81 were highly expressed in iPSCs (Figure 1B).

Next, we tested the ability of iPSC lines to form tissues of all three embryonic germ layers in mice. Subcutaneous, intramuscular, and intratesticular injections of six iPSC lines were performed in immunodeficient mice. Teratoma formation was observed 4–8 weeks later. Histological evaluation of the tumors revealed abundant differentiation into epithelia of all three embryonic germ layers. Figure 2B shows representative images of respiratory ciliated epithelium (endoderm), cartilage epithelium (mesoderm), and pigmented neuroectodermal epithelium (ectoderm). The in-vivo-derived tumors showed endodermal-specific markers α-fetoprotein and GATA4, the mesodermal-specific markers α-major histocompatibility complex (MHC) and BRACHYURY, and ectodermal-specific markers β-III-tubulin and vimentin (Figure 2A).

Cardiac Differentiation

Spontaneously beating clusters of cells first appeared around day 7 postinitiation of differentiation using the matrix sandwich protocol (see Experimental Procedures). By flow cytometry, 65%–90% of cells stained positive for α-actinin at 15 days postdifferentiation (Figure 3A). Immunocytochemistry staining of hiPS-CM revealed the typical pattern of sarcomeric structures and organization (Figure 3B). Further functional characterization of the hiPSC CM is described in the following sections.

Electrophysiological Properties of Single CMs Differentiated from PBMC iPSCs

Action potentials (APs) were recorded from single-beating CMs between 30 and 50 days postdifferentiation using the disrupted patch technique (see Experimental Procedures). Similar to cardiac myocytes differentiated from human ESCs and human fibroblast-derived iPSCs (Itzhaki et al., 2011; Lahti et al., 2012; Liang et al., 2013; Navarrete et al., 2013; Yazawa et al., 2011), myocytes differentiated from PBMC-derived iPSCs demonstrated distinct AP properties that can be arbitrarily categorized as nodal-, atrial-, and ventricular-like (Figure 4). Nodal-like myocytes were characterized by a more depolarized maximum diastolic potential (MDP) and slower upstroke velocity compared with atrial- and ventricular-like myocytes. Atrial-like myocytes were distinguished by shorter APD and slower upstroke velocities compared to ventricular-like myocytes. Ventricular-like myocytes displayed the longest APD (measured at 10%, 50%, and 90% of repolarization), lowest resting membrane potential, and the fastest upstroke velocities. All three types of myocytes displayed spontaneous beating at similar cycle lengths. The spontaneous depolarization and relatively depolarized MDP of the iPSC-derived myocytes are consistent with the immature nature of these cells and are similar to the properties described for myocytes differentiated from ESC lines and fibroblast-derived iPSCs (Itzhaki et al., 2011; Lahti et al., 2012; Liang et al., 2013; Navarrete et al., 2013; Yazawa et al., 2011). The sample size of

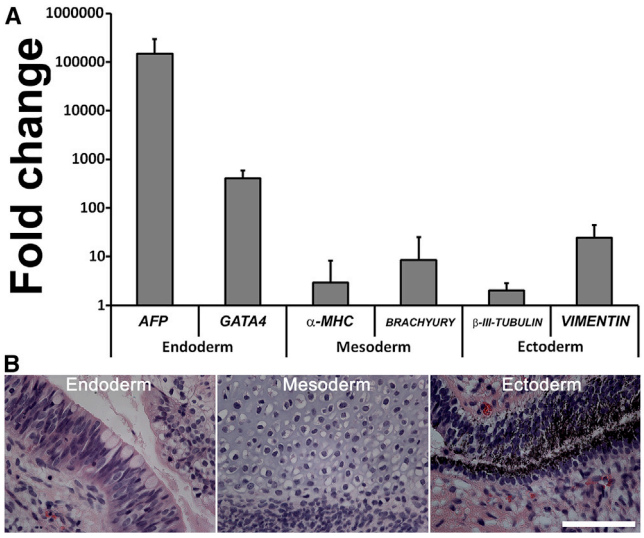

Figure 2. Ability of Human PBMC-Derived iPSCs to Differentiate into Cells of All Three Embryonic Germ Layers

(A) Quantification of the expression of representative genes of the three embryonic germ layers. The relative expression of AFP, GATA4 (both endoderm), α-MHC, BRACHYURY (both mesoderm), β-III-tubulin, and vimentin (both ectoderm) is shown in relation to undifferentiated hiPSCs from the same patient. Error bars, SD (n = 4 independent experiments).

(B) Teratoma, derived from hiPSCs comprising cell types of all three embryonic germ layers. Representative images show respiratory ciliated epithelium (endoderm), cartilage epithelium (mesoderm), and pigmented neuroectodermal epithelium (ectoderm). Scale bar, 100 μm.

CMs selected for patch-clamp analysis was relatively small and therefore may not represent the true distribution of CM subtypes.

Electrophysiological Properties of CM Monolayers Differentiated from PBMC iPSCs

To assess the electrical coupling of the hiPSC-derived CMs, we seeded terminally differentiated CMs on MEA chambers and measured spontaneous cycle length, repolarization properties, and conduction velocity in three iPSC lines derived from patient hB53 (Figure 5A). Local electrograms revealed high-fidelity depolarization and repolarization waves that allowed for the precise measurement of the ARI and conduction velocity across the array (Figure 5A).

Analysis of all 60 electrograms combined allowed for creation of isochronal maps of activation time (AT), ARI, and conduction velocity across the array (Figures 5B and 5C; Figure S1 available online). There were no differences in spontaneous cycle lengths and conduction velocities between myocytes from the three iPSC lines. Moreover, there was no difference in mean ARI values between arrays plated with myocytes differentiated from three distinct iPSC lines. However, as expected for a heterogeneous population of myocytes, there was heterogeneity in repolarization across the array, as measured by the ARI. The ARI measurement is a direct correlate of APD50 (see Discussion; Chinushi et al., 2001; Fuller et al., 2000b; Haws and Lux, 1990) and thus is comparable to the APD50 values listed in Figure 4 (70, 137, and 310 ms for nodal-, atrial-, and ventricular-like cells, respectively, compared to the mean ARI of ~180 ms). The mean ARI value observed is a composite value that likely reflects electrotonic coupling between individual cells of varying APD. We previously showed that direct coupling of myocytes of varying AP morphology and APD results in an intermediate, composite AP (Spitzer et al., 1997). However, the relative contribution of chamber-specific myocytes to the mean ARI cannot be definitively ascertained by MEA analysis.

Next, we tested the effects of various antiarrhythmic agents on the electrophysiological properties of iPSC CM (Figure 6). Lidocaine (LIDO) caused a dose-dependent prolongation of repolarization that was reversible with washout. The higher LIDO concentrations (≥100 μM) likely caused a block of rapidly activating delayed rectifier potassium current (I_{Kr}) that, in turn, resulted in delayed repolarization. LIDO also resulted in progressive slowing of conduction velocity, confirming the role of Na^+ channels in impulse propagation in hiPSC-derived CMs. Although conduction velocity achieved statistical significance only for the 100 μM dose, there was a trend toward slower velocity at higher LIDO concentrations, compared to control. Dofetilide caused a dose-dependent prolongation of the ARI, underscoring an important role for I_{Kr} in meditating repolarization in CMs differentiated from PBMC-derived iPSCs. Higher concentrations of dofetilide induced secondary depolarizations indicative of early-after depolarizations (EADs) (Figure S2). The effects of dofetilide were irreversible (data not shown). Diltiazem caused dose-dependent shortening of repolarization and a marked increase in spontaneous cycle length. The diltiazem-induced slowing of spontaneous beating indicates a role for L-type Ca^{2+} in firing rate, as is typical for pacemaker cells and embryonic CMs. Finally, amiodarone did not alter repolarization, spontaneous cycle length, or conduction velocity even at concentrations up to 1 mM. The dose-dependent drug effects were similar within myocytes derived from the three iPSC lines. Taken together, these data demonstrate that cardiomyocytes differentiated from PBMC-derived iPSCs display electrophysiological characteristics of immature myocytes, respond to prototypical antiarrhythmic agents in an expected manner, and behave similar to myocytes differentiated from fibroblast-derived iPSCs. Moreover, myocytes differentiated from distinct iPSC lines from a single patient share similar electrophysiological properties and drug responses.

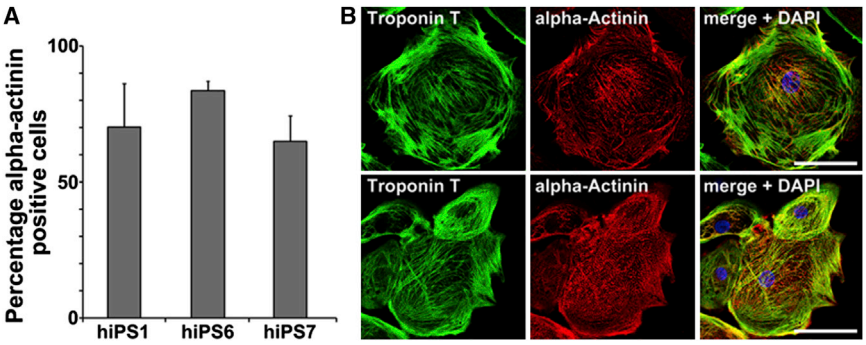

Figure 3. Human PBMC-Derived iPSCs Give Rise to Functional CMs

(A) High percentage of α-actinin-positive cells. After differentiation, cells were stained for the cardiac marker protein α-actinin and analyzed by a flow cytometer. Depending on the hiPSC line, up to 87% of the cells were positive for α-actinin (line hB53 hiPS6). Error bars, SD (n = 3 independent experiments).

(B) Representative images of troponin T- and α-actinin-stained hiPSC-derived CMs. Scale bars, 10 μm (upper panel) and 30 μm (lower panel).

Rapid Electrical Stimulation Induces Electrical Remodeling in Cultured CMs Differentiated from Human PBMC-Derived iPSCs

Next, we tested the effects of rapid electrical stimulation (tachypacing) on calcium handling in CMs differentiated from human PBMC-derived iPSCs in culture. CM clusters were stimulated at 1 and 4 Hz for 1, 4, 8, and 12 hr. CMs did not tolerate 12 hr of electrical stimulation at a rate of 4 Hz. These cells developed blebbing of the cell membrane by light microscopy and were not further analyzed. No differences in CaT parameters were detected in myocytes stimulated for 4 hr compared to nonpaced control cells (Figure S3). However, rapid stimulation at 4 Hz for 8 hr dramatically reduced Ca^{2+} transient magnitude and slowed the rate of transient decay, compared to cells paced at 1 Hz and unpaced controls (Figure 7). In addition, CaTs recorded from cells stimulated at 4 Hz for 8 hr displayed abnormal secondary Ca^{2+} releases. Rapid electrical stimulation reduced L-type Ca^{2+} channel transcripts, as measured by real-time qPCR. These results indicate that hiPSC CMs undergo acute electrical remodeling in response to tachypacing, similar to that described in other in vitro and in vivo models of tachycardia.

DISCUSSION

The ability to generate patient-specific CMs from somatic cells is revolutionizing the study of cardiovascular diseases and holds tremendous promise for drug discovery, toxicology screening, and personalized medicine approaches. Although a skin biopsy to obtain dermal fibroblasts is considered minimally invasive, a blood draw is a far simpler and more acceptable approach to obtain somatic cells for reprogramming, especially in the pediatric population. Although the majority of reprogramming studies have focused on fibroblasts as the somatic cell source, several studies have recently demonstrated the feasibility of reprogramming PBMCs. IPSCs derived from PBMCs have been successfully differentiated into mesenchymal stems cells, hepatocytes, and CMs (Brown et al., 2010; Churko et al., 2013; Sommer et al., 2012; Staerk et al., 2010). However, to date, there has been no comprehensive characterization of the electrophysiological properties of CMs differentiated from human PBMC-derived iPSCs. Here, we describe the electrophysiological and pharmacological characterization of CMs differentiated from human PBMC-derived iPSCs.

CMs differentiated from PBMC-derived iPSCs demonstrated the typical AP features and morphologies consistent with nodal-, atrial-, and ventricular-like phenotypes. The specific electrophysiological features, including MDP, upstroke velocity, and APD10, APD50, and APD90, for the three cell types were generally similar to values reported for CMs differentiated from fibroblast-derived iPSCs and ESCs (Itzhaki et al., 2011; Lahti et al., 2012; Liang et al., 2013; Navarrete et al., 2013; Yazawa et al., 2011). We were surprised at the similarity in AP parameters given the distinct source of somatic cells and differences in the experimental conditions. These observations suggest that despite the reported differences in epigenetic memory between different somatic cell sources, the electrophysiological behavior of the differentiated human CMs remains remarkably similar.

MEAs offer the potential for moderate-throughput characterization of the electrophysiological and pharmacological properties of iPSC-derived CMs. Analysis of the pharmacological effects of various antiarrhythmic agents provides additional insight into the underlying electrophysiology of these CMs. For example, the slowing of conduction velocity by LIDO indicates an essential role for Na^{+} channels in impulse propagation, an important feature of mature CMs. Moreover, the sensitivity of diltiazem to slow the spontaneous cycle length is consistent with the known role for L-type Ca^{2+} channels in modulating pacemaker activity. Interestingly, we found no specific alterations in the measured electrophysiological parameters in response to increasing concentrations of amiodarone.

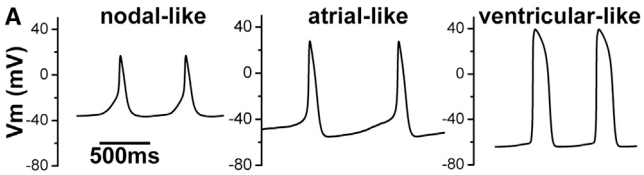

B

APs (n =27)	CL (s)	MDP (mV)	P_{max} (mV/s)	APD_{10} (ms)	APD_{50} (ms)	APD_{90} (ms)
Nodal-like (n=8)	1.1±0.12	-42.4±2.5*	8.4±1.1*	33.0±4.5*	73.2±6.1*	138.5±15.1*
Atrial-like (n=11)	1.01±0.10*	-60.2±1.5*	11.2±0.8*	67.6±6.7*	156.2±13.2*	212.3±14.0*
Ventricular-like (n=8)	1.40±0.05*	-68.6±2.3*	56.9±9.5*	111.8±6.9*	309.5±16.6*	413.7±28.2*

Figure 4. APs Recorded from CMs Differentiated from Human PBMC-Derived iPSCs

(A) Representative APs recorded from individual myocytes displaying nodal-, atrial-, and ventricular-like phenotypes.

(B) Table displaying AP parameters for the three subtypes of CMs. CL, cycle length (s); MDP, in mV; Pmax, maximum upstroke velocity (mV/ms); APD10, APD50, or APD90, APD at 10%, 50%, or 90% of repolarization (ms). Values are mean ± SEM. *p < 0.05 (ANOVA with Bonferroni correction). All three subgroups were different from each other for the measured parameters, except CL, where only atrial- and ventricular-like groups were statistically different. The "n" listed in the table represents independent recordings from CMs differentiated from iPSC line C1.

Although considered a class III antiarrhythmic agent, amiodarone's effects are complex and vary with respect to acute and chronic administration. There is considerable variation in the degree of APD modulation induced by acute exposure to amiodarone, with reports of shortening, prolongation, and no effect on APD (Kodama et al., 1997). Acute amiodarone blocks inward Na^+ and Ca^{2+} currents as well as delayed rectifier K^+ currents, and some of the effects are rate dependent (Kato et al., 1988; Kodama et al., 1996). We speculate that the multiple channel and receptor-blocking effects of amiodarone result in competing effects that ultimately cause no net change in our measured MEA parameters. Finally, ARI prolongation and the induction of triggered depolarizations by dofetilide underscore the importance of I_{Kr} in repolarization of CMs.

The pharmacological effects of antiarrhythmic agents in PBMC-derived iPSC CMs described here are similar to those reported for CMs differentiated from fibroblast-derived iPSCs (Braam et al., 2013; Liang et al., 2013; Navarrete et al., 2013). These observations further support the notion that epigenetic memory based on the somatic cell source may not have important functional consequences for iPSC-derived CMs, with respect to basic electrophysiology. Whether epigenetic memory plays an important role in other physiologic or metabolic processes remains to be determined. In addition, we found that individual iPSC lines derived from the same patient displayed similar electrophysiological features and pharmacological responses. These findings have important implications for determining how many cell lines are necessary for proper characterization of disease-specific iPSC-based models of cardiovascular disease.

MEA-based analyses are an important tool to characterize patient- or disease-specific responses to pharmacological interventions and provide a platform for in vitro preclinical screening for QT interval-prolonging drugs. As such, proper measurement of repolarization is critical for the accurate determination of risk assessment for drug development and a mechanistic understanding of arrhythmia models. The extracellular field potential is determined by the transmembrane currents that shape the AP of individual cells within the vicinity of the electrode. However, the currently accepted standard measures of repolarization do not precisely relate to *local* repolarization at the level of the transmembrane AP. For example, most published stem cell-derived myocyte studies report the time at the "end" of the repolarization wave (field potential duration), as if one were measuring the end of a T wave on a surface electrocardiogram (ECG) (Itzhaki et al., 2011, 2012; Lahti et al., 2012; Liang et al., 2013; Malan et al., 2011; Matsa et al., 2011; Moretti et al., 2010; Navarrete et al., 2013; Yazawa et al., 2011). Alternatively, the time to peak of the repolarization wave is reported (Zwi et al., 2009). Although both measurements track repolarization in a general sense, neither reflects an accurate correlate of local APD. Moreover, despite the lack of any data supporting its applicability, the Bazett correction factor is often applied to the field potential duration measurement to correct for cycle length changes. By contrast, the ARI is an established measure of local repolarization that has been extensively validated in animal models and human studies, using simultaneously acquired intracellular recordings and monophasic APD recordings (Ajijola et al., 2013; Chinushi et al., 2001; Compton et al., 1996; Fuller et al., 2000a, 2000b; Haws and Lux, 1990; Nosten et al., 1993; Vaseghi et al., 2013; Yue et al., 2004). The ARI directly correlates with the duration between the times of steepest transmembrane AP upstroke and downstroke (Chinushi et al., 2001; Fuller et al., 2000b; Haws and Lux, 1990). The steepest portion of phase 3 AP repolarization reflects the timing of APD50 and is expressed in local electrograms (field potentials) as the time of steepest upstroke of the T wave. Thus, ARI measurements have a direct correlate with transmembrane APs (i.e., APD50) in cells local to the recording electrode, as opposed to field potential duration, a *global* assessment that reflects the time at which all cells across the electrode array have repolarized. Based on our work here and published elsewhere (Ajijola et al., 2013; Chinushi et al., 2001; Compton et al., 1996; Fuller et al., 2000a, 2000b; Haws and Lux, 1990; Nosten et al., 1993; Vaseghi et al., 2013; Yue et al., 2004), we

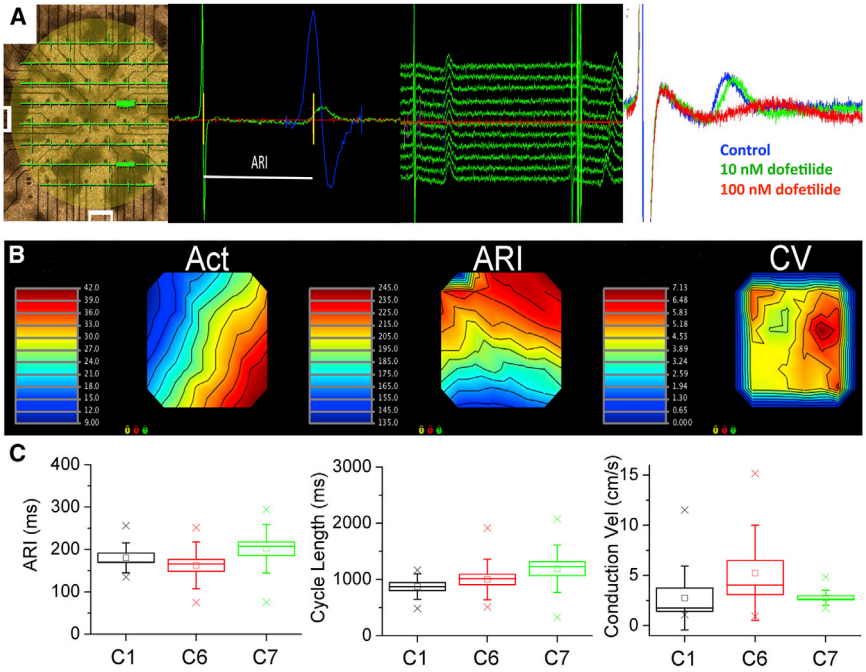

Figure 5. Electrophysiological Properties of hiPSC CMs as Measured Using a 60-Electrode MEA Chamber

(A) Left, image of the 60-electrode MEA system, plated with monolayer of hiPSC CM. Superimposed on the image are the individual electrograms recorded at each electrode position. Center-left view is an example of methodology used to calculate the ARI. Green trace represents a single beat recorded at one lead of the MEA, showing depolarization and repolarization complexes, reminiscent of QRS and T waves. The ARI is calculated as time between the minimum first derivative of voltage (dV/d*t*) in the depolarization wave and the time of maximum dV/d*t* near the peak of the repolarization wave (bounded by the yellow lines). Blue trace represents dV/d*t* curve of the repolarization wave, used to determine maximum dV/d*t*. Center-right view shows example traces of consecutive spontaneous beats recorded at a single MEA site. ARIs for each lead were averaged to obtain a mean ARI value at each site for the duration of the recording. Right view is a representative electrogram recorded under control conditions and after perfusion with 10 and 100 nM dofetilide. Note the prolongation of the repolarization wave with increasing concentrations of dofetilide.

(B) Isochronal time maps from a typical MEA chamber demonstrating AT (Act) across the array, ARI (a surrogate for APD), and conduction velocity (CV). Act and ARI are reported in ms. CV is reported as cm/s.

(C) CMs differentiated from three different iPSC lines (C1, C6, and C7) exhibit similar electrophysiological properties. Box plots show mean (square), SEM (box), SD (error bars), and 95% confidence intervals (crosshatch). No significant differences were detected within cell lines with respect to the ARI, cycle length, and conduction velocity (n = 10–13 independent recordings).

propose the ARI as the gold standard measure of repolarization to most accurately define in vitro repolarization in MEA analyses of iPSC CMs.

Finally, here, we report the application of hiPSC CM to a powerful model system for the study of arrhythmia susceptibility and mechanisms based on a tachypacing system pioneered for use in an atrial tumor cell line. Rapid stimulation (in vitro tachypacing) of cultured HL-1 atrial myocytes induces acute electrical remodeling similar to that reported from in vivo tachypacing models and human atrial arrhythmia (Brundel et al., 2001, 2004, 2006; Ke et al., 2011; Mace et al., 2009; Qi et al., 2008; Yang et al., 2005). The hallmark of electrical remodeling is an abrupt reduction in L-type Ca^{2+} current as a consequence of downregulation of $Ca_v1.2$ mRNA and proteins (Shiroshita-Takeshita et al., 2005). Likewise, we observed an acute decrease in CaT amplitude and $Ca_v1.2$ mRNA in response to rapid electrical stimulation, supporting the notion that hiPSC CMs also undergo acute electrical remodeling. It is worth noting that our cells are heterogeneous in nature, encompassing a mixture of nodal-, atrial-, and ventricular-like cells. Despite this caveat, our study provides a preliminary description of acute electrical remodeling in hiPSC-derived myocardial cells. Future studies will characterize in detail the molecular processes that underlie acute electrical remodeling in iPSC CMs linked to acquired and/or inheritable human diseases.

Limitations

Several limitations are inherent to any hiPSC-CM study, given the current state of research in this field. Although efforts are ongoing to bias differentiation into chamber-specific lineages (Zhang et al., 2011), there is currently no established method for separating iPSC CMs into atrial- or ventricular-specific subgroups. Moreover, the designation of nodal-, atrial-, and ventricular-like CMs is somewhat arbitrary, based on qualitative analysis of AP waveforms, thus further complicating methods to isolate chamber-specific lineages. Purification of atrial- or ventricular-specific cell lines is necessary to advance the study of chamber-specific diseases, such as atrial fibrillation or ventricular tachycardia. The relatively immature nature of hiPSC CMs is also a limitation of this model system, complicating extrapolation to disease mechanism in adult myocardium. Recent reports indicate that increasing the

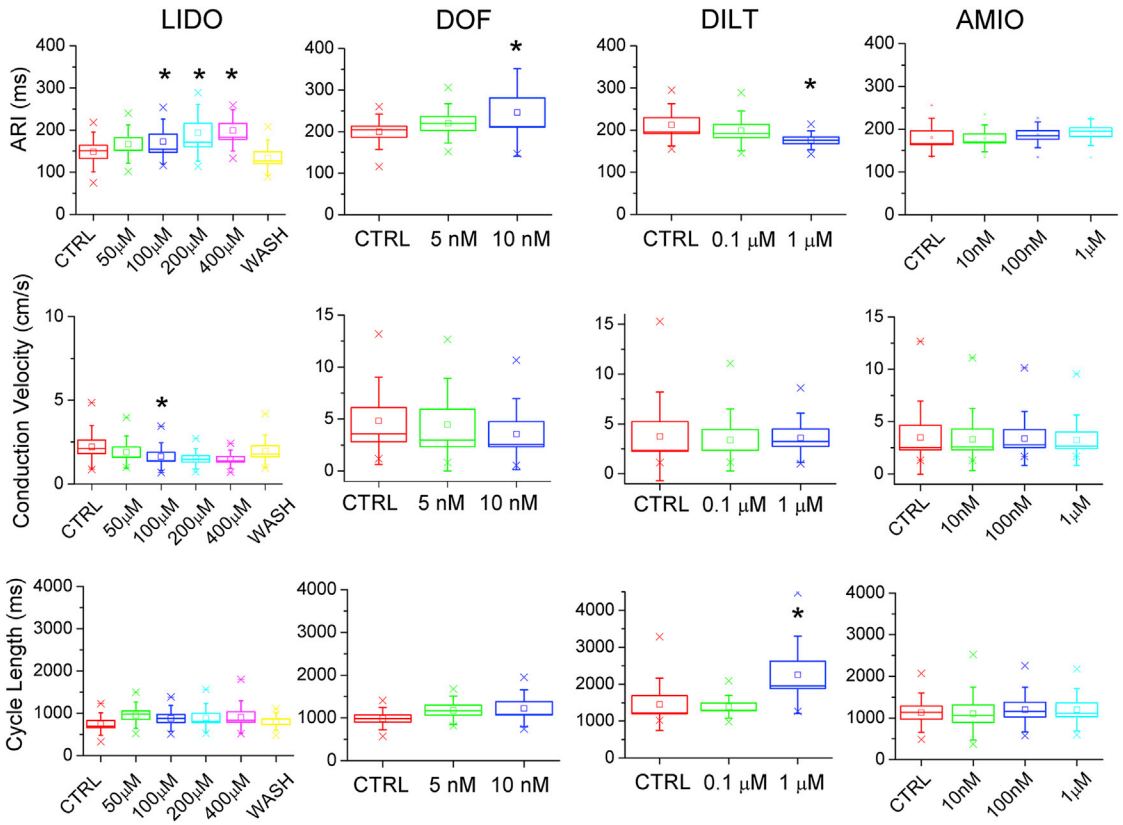

Figure 6. The Electrophysiological Effects of Various Antiarrhythmic Agents on CMs Differentiated from Human PBMC-Derived iPSCs

hiPSC-CM monolayers plated on MEA chambers were perfused with sequential concentrations of LIDO, dofetilide (DOF), diltiazem (DILT), and amiodarone (AMIO). The ARI, conduction velocity, and cycle length were measured. *$p < 0.05$, calculated using repeated-measures ANOVA with Bonferroni correction. CTRL, control; WASH, washout. n = 10 (LIDO and DOF) and 9 (DILT and AMIO) independent experiments.

duration of iPSC-CM culture promotes maturation (Ivashchenko et al., 2013). Finally, an important limitation was our inability to pace hiPSC CMs when cultured on the MEA chamber. Thus, we were unable to characterize the relationship between cycle length and the ARI to determine whether cycle length correction is necessary in this model system. APD of individual myocytes shortens with faster cycle lengths (unpublished data), and thus, we speculate that a rate correction factor for MEA analyses is necessary to precisely determine drug effects on repolarization in the setting of altered spontaneous cycle lengths.

Conclusions

In summary, our data indicate that electrophysiological properties and pharmacological responses of PBMC-derived iPSC CMs are generally similar to those of iPSC CMs derived from other somatic cells, suggesting that epigenetic memory may not play an important functional role in iPSC CMs. We also show that CMs differentiated from distinct iPSC lines from a single patient display similar electrophysiological features and pharmacological responses. Finally, we demonstrate that hiPSC CMs undergo acute changes in calcium-handling properties and gene expression in response to rapid electrical stimulation, laying the foundation for an in-vitro-tachypacing model system for the study of human tachyarrhythmias.

EXPERIMENTAL PROCEDURES

hiPSC Generation and CM Differentiation

All human subject research was approved by the University of Utah institutional review board. After obtaining informed consent, peripheral blood was obtained from a 25-year-old Caucasian male (patient hB53), and PBMCs were isolated by density gradient centrifugation (So et al., 2013). To induce reprogramming and increase the infection efficiency of PBMCs, cells were infected with lentiviruses expressing OCT4, KLF4, SOX2, and c-MYC from a polycistronic cassette (pHAGE2-TetOminiCMV-hSTEMCCA) (Sommer et al., 2010; Staerk et al., 2010). We employed two rounds of lentiviral spin infection (day 9 and day 10) in which PBMCs were simultaneously infected with constitutively active lentiviruses encoding

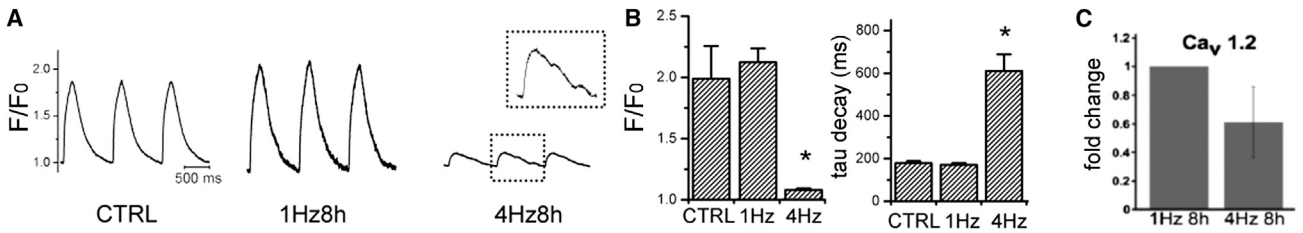

Figure 7. Rapid Electrical Stimulation Reduces Ca^{2+} Transients and Cav1.2 Expression in hiPSC CM

(A) Representative Ca^{2+} transients recorded using fluo-4-labeled hiPSC CMs unpaced (CTRL) and paced at 1 or 4 Hz for 8 hr. Note the abnormal secondary Ca^{2+} release during decay phase (inset).

(B) Bar graphs showing magnitude of Ca^{2+} transient expressed as F/F_0 and rate of transient decay (tau, ms). *$p < 0.0001$ compared to 1 Hz and CTRL. n = 10 independent recordings, each group.

(C) Cav1.2 expression, measured by RT-qPCR, in hiPSC CMs subjected to 1 and 4 Hz electrical stimulation.

the reverse tetracycline transactivator (FUW-M2rtTA) (Hockemeyer et al., 2008) and the STEMCCA vector. Infected blood cells were transferred onto mouse embryonic fibroblast (MEF) feeder cells 3 days postinfection and cultured for an additional 7 days in MEF medium supplemented with 10 ng/ml basic human fibroblast growth factor, 5 mg/ml ascorbic acid, and 2 mg/ml doxycycline. Following the appearance of small colonies, the medium was changed to human ESC medium: Dulbecco's modified Eagle's medium/F12 supplemented with GlutaMAX, 10 mM NEAA, 25 U/ml penicillin, 25 μg/ml streptomycin, 100 μM β-mercaptoethanol, and 20% knockout serum replacement (Invitrogen) with 10 ng/ml basic fibroblast growth factor and 2 mg/ml doxycycline. Colonies were selected and expanded around day 30 postinfection. After three passages on MEF feeder cells, the iPSC clones were transferred to Matrigel (BD Biosciences; #354277)-coated dishes, cultured, and expanded in mTeSR1 according to the manufacturer's protocol and gradually tapered from doxycycline.

CM differentiation was achieved by the matrix sandwich method developed by Kamp and colleagues (Zhang et al., 2012; J. Zhang et al., 2010, Circulation, abstract). The iPSCs were grown as a monolayer in an artificial extracellular matrix and sequentially treated with growth factors known to be involved in early embryonic heart development (activin A and bone morphogenic protein-4) (Zhu et al., 2011). In practice, the iPSCs were seeded as a monolayer on Matrigel-coated dishes in mTeSR1 (or Essential 8), followed by a Matrigel overlay in RPMI plus B27 (-insulin) (Invitrogen) medium, and sequential treatment with activin A, bone morphogenic protein-4, and basic human fibroblast growth factor.

Quantitative Real-Time PCR

Total mRNA was harvested from PBMCs, iPSC clones, and contracting hiPSC CMs (Ambion; PureLink RNA Kit), and cDNA was synthesized (Applied Biosystems; High-Capacity cDNA Reverse Transcription Kit). Gene expression was quantified by RT-qPCR using primers (see Tables S1 and S2) and SYBR Green from QIAGEN in an Applied Biosystems 7900HT thermocycler. Expression levels were normalized to 18S rRNA.

Immunocytochemistry

Immunocytochemistry was performed on iPSCs or hiPSC CMs using standard protocols with the primary antibodies listed in Table S3. Cells were incubated with the following secondary antibodies: Alexa Fluor 555 donkey anti-mouse or anti-rabbit immunoglobulin G (IgG) (1:2,000; Invitrogen); Alexa Fluor 488 donkey anti-rabbit IgG (1:2,000; Invitrogen); and Alexa Fluor 488 goat anti-mouse IgG (1:2,000; Invitrogen). Nuclei were detected with DAPI (Vector Laboratories; VECTASHIELD H-1200).

Teratoma Formation and Analysis

Teratomas were generated by injecting undifferentiated iPSCs into nonobese diabetic severe combined immunodeficiency (SCID) mice. Undifferentiated iPSCs were dissociated into single cells, and approximately 1.5 million cells were injected into the testis and/or the gastrocnemius muscle of the mice. Teratomas were collected 4–8 weeks postinjection, then fixed with 10% zinc formalin and embedded in paraffin.

Karyotype Analysis

Karyotype analysis was performed at ARUP Laboratories (Salt Lake City). The iPSCs (at 70% confluence) were collected in hypotonic potassium chloride (KCl) solution, fixed in methanol:glacial acid 3:1, plated on microscope slides, then stained with Leishman's stain. Metaphase spreads for each sample were analyzed.

Flow Cytometry

Enzymatically dissociated iPSCs were blocked, then reconstituted in fluorescence-activated cell sorting (FACS) buffer (PBS plus 5% fetal calf serum) containing the primary antibodies listed in the Table S3. For secondary staining, cells were resuspended in FACS buffer containing 1:500 diluted Alexa Fluor 488 and/or Alexa Fluor 647-conjugated antibodies (Invitrogen; #A11017 or #A31573, respectively). Flow cytometry was performed on a BD Biosciences FACSCanto II using 488 and 635 nm lasers. Data analysis was done with FlowJo (TreeStar). Isotype controls were used to set gates for positive and negative populations.

Electrophysiological Characterization of hiPSC-Derived CMs

AP Recordings

Spontaneously beating hiPSC CMs from patient hB53 (days 30–50 postdifferentiation) were studied. Cells were plated at low density

to increase the likelihood of observing single, beating myocytes. All experiments were performed at 37°C. The recording chamber was superfused with a buffered, physiological solution containing 126 mmol/l NaCl, 4.4 mmol/l KCl, 1.1 mmol/l $CaCl_2$, 1 mmol/l $MgCl_2$, 11 mmol/l glucose, and 24 mmol/l HEPES (pH 7.4 with NaOH). Electrodes made from borosilicate capillary tubes (#8250 capillary glass; A-M Systems) were fire polished to obtain resistances of 6–9 MΩ filled with internal solution containing 120 mmol/l KCl, 5 mmol/l EGTA, 5 mmol/l K_2ATP, 5 mmol/l $MgCl_2$, and 10 mmol/l HEPES (pH 7.2).

Transmembrane potential (V_m) was measured by using an AxoClamp 2A amplifier (Molecular Devices) in the bridge mode with the disrupted patch technique. V_m was filtered at 10 kHz and digitized at a sampling frequency of 20 kHz with a 12-bit analog-to-digital converter (Digidata 1322A Interface; Molecular Devices). The following AP parameters were analyzed: MDP, peak maximum upstroke velocity, amplitude, and APD. APD was calculated as the time interval between the peak maximum upstroke velocity (phase 0) and the time at 10% (APD10), 50% (APD50), and 90% (APD90) of repolarization.

Recording of Extracellular Field Potential from Monolayers of hiPS-CM

To characterize the electrophysiological properties of hiPSC CMs, the cells were plated onto a MEA recording chamber (MEA60-System; Multi Channel Systems) treated with fibronectin. Each MEA chamber consisted of 60 surface electrodes, with a recording field of 1.4 × 1.4 mm. Cells were superfused with buffered physiological solution (see above) at 37°C. Spontaneous extracellular field potentials were recorded (5 kHz/channel sampling rate) from electrodes across the array.

Local APD at each electrode was estimated by measuring the ARI. The utility of the ARI as a surrogate for APD has been extensively validated in animal models and human studies (Chinushi et al., 2001; Fuller et al., 2000a; Haws and Lux, 1990; Yue et al., 2004) using simultaneously acquired intracellular recordings and monophasic APD recordings. In each electrogram, AT was measured as the time of minimum first derivative of voltage (dV/d*t*) in the depolarization wave and repolarization time measured as the time of maximum dV/d*t* near the peak of the repolarization wave. The ARI was measured as the difference between repolarization and ATs and reflects the local APD at the electrode site. Data from all channels were analyzed using a custom-written program with a graphic user interface. Color-coded isochronal maps were constructed using a standard 2D plotting routine based on the local ATs between electrodes. Conduction velocity vectors were calculated at each individual electrode, and the average conduction speed in the monolayer was calculated from the individual velocity vectors as the mean of the conduction speed (magnitude of velocity vector).

In order to assess the quality of the MEA data, we plotted the cumulative probability distribution functions (CPDFs) of AT and ARI values for each spontaneous beat (typically 12–20 beats/recording) in each of the 60 electrograms. These plots allow for an assessment of the quality of the data by highlighting outlier measurements that might skew the average calculation (Figure S1). A steep slope of the CPDF relationship indicates that values for all beats were very similar, whereas a shallow slope indicates a wide variation in measured parameters. We calculated the average AT and ARI value while excluding 20% of the measurements at the extremes.

Pharmacological Evaluation Using MEA Recordings

Electrophysiological effects of antiarrhythmic agents including diltiazem, amiodarone, dofetilide, and LIDO on CMs cultured in monolayers were evaluated using the MEA system. Dose-response experiments were repeated in triplicate for three different hiPS-CM lines generated from patient hB53. The hiPSC CMs were superfused with buffered physiological solution at 37°C containing increasing concentrations of the study drug while spontaneous extracellular field potentials were recorded. The cells were perfused with the study drug for 5 min to achieve quasi-steady state before acquiring data.

Measurement of Intracellular Calcium

CaTs were detected in hiPSC CMs with an epifluorescence system using the fluorescent indicator fluo-4 AM (Molecular Probes). Details are described in the Supplemental Experimental Procedures.

Rapid Electrical Stimulation of hiPSC CM in Culture

Small clusters of spontaneous contracting hiPSC CMs were isolated and maintained in RPMI plus B27 (+insulin) media, then plated on six cell culture dishes. Cells were electrically stimulated using carbon electrodes immersed in the culture media (C-Dish; IonOptix), connected to a custom-built electrical stimulator via a ribbon cable. This system allowed for cells to be electrically stimulated while housed inside the incubator. Cells were electrically paced at 1 and 4 Hz for 8 hr, using bipolar square-wave pulses of 5–15 ms duration and an amplitude of 20 V. To ensure effective "capture" of pacing, current and pulse duration were adjusted until visible contractions were synchronous with the pacing frequency. Effective capture was reassessed visually throughout the stimulation period.

Statistics

Differences in electrophysiological parameters in response to increasing concentrations of antiarrhythmic agents were tested using repeated-measures ANOVA (SYSTAT 13; Systat Software) and the Bonferroni correction. Nonpaired measurement differences were tested using ANOVA. A p value <0.05 was required for statistical significance.

SUPPLEMENTAL INFORMATION

Supplemental Information includes Supplemental Experimental Procedures, three figures, and three tables and can be found with this article online at http://dx.doi.org/10.1016/j.stemcr.2014.04.017.

AUTHOR CONTRIBUTIONS

M.R., C.J.J., R.L.L., A.P.M., K.W.S., M.T.-F., and I.J.B. designed experiments. M.R., C.J.J., S.L., A.P.M., K.W.S., E.C., and M.T.-F. performed experiments and analyzed data. R.L.L. analyzed data. M.R., C.J.J., M.T.-F., and I.J.B. wrote the paper.

ACKNOWLEDGMENTS

This work was supported by the Nora Eccles Treadwell Foundation (to M.T.-F., K.W.S., and A.P.M.), the American Heart Association

(to C.J.J.), the NHLBI 2009 NIH Director's Pioneer Award 7 DP1 HL117650-05 (to I.J.B.), VA Merit Review Award (to I.J.B.), NHLBI 5R01HL074370-04 (to I.J.B.), and NIH Merit Award R37 HL042873-24 (to K.W.S.).

Received: March 14, 2014
Revised: April 28, 2014
Accepted: April 29, 2014
Published: May 29, 2014

REFERENCES

Ajijola, O.A., Yagishita, D., Patel, K.J., Vaseghi, M., Zhou, W., Yamakawa, K., So, E., Lux, R.L., Mahajan, A., and Shivkumar, K. (2013). Focal myocardial infarction induces global remodeling of cardiac sympathetic innervation: neural remodeling in a spatial context. Am. J. Physiol. Heart Circ. Physiol. *305*, H1031–H1040.

Braam, S.R., Tertoolen, L., Casini, S., Matsa, E., Lu, H.R., Teisman, A., Passier, R., Denning, C., Gallacher, D.J., Towart, R., and Mummery, C.L. (2013). Repolarization reserve determines drug responses in human pluripotent stem cell derived cardiomyocytes. Stem Cell Res. (Amst.) *10*, 48–56.

Brown, M.E., Rondon, E., Rajesh, D., Mack, A., Lewis, R., Feng, X., Zitur, L.J., Learish, R.D., and Nuwaysir, E.F. (2010). Derivation of induced pluripotent stem cells from human peripheral blood T lymphocytes. PLoS ONE *5*, e11373.

Brundel, B.J., Van Gelder, I.C., Henning, R.H., Tuinenburg, A.E., Wietses, M., Grandjean, J.G., Wilde, A.A., Van Gilst, W.H., and Crijns, H.J. (2001). Alterations in potassium channel gene expression in atria of patients with persistent and paroxysmal atrial fibrillation: differential regulation of protein and mRNA levels for K+ channels. J. Am. Coll. Cardiol. *37*, 926–932.

Brundel, B.J., Kampinga, H.H., and Henning, R.H. (2004). Calpain inhibition prevents pacing-induced cellular remodeling in a HL-1 myocyte model for atrial fibrillation. Cardiovasc. Res. *62*, 521–528.

Brundel, B.J., Henning, R.H., Ke, L., van Gelder, I.C., Crijns, H.J., and Kampinga, H.H. (2006). Heat shock protein upregulation protects against pacing-induced myolysis in HL-1 atrial myocytes and in human atrial fibrillation. J. Mol. Cell. Cardiol. *41*, 555–562.

Chinushi, M., Tagawa, M., Kasai, H., Washizuka, T., Abe, A., Furushima, H., and Aizawa, Y. (2001). Correlation between the effective refractory period and activation-recovery interval calculated from the intracardiac unipolar electrogram of humans with and without dl-sotalol treatment. Jpn. Circ. J. *65*, 702–706.

Churko, J.M., Burridge, P.W., and Wu, J.C. (2013). Generation of human iPSCs from human peripheral blood mononuclear cells using non-integrative Sendai virus in chemically defined conditions. Methods Mol. Biol. *1036*, 81–88.

Compton, S.J., Lux, R.L., Ramsey, M.R., Strelich, K.R., Sanguinetti, M.C., Green, L.S., Keating, M.T., and Mason, J.W. (1996). Genetically defined therapy of inherited long-QT syndrome. Correction of abnormal repolarization by potassium. Circulation *94*, 1018–1022.

Fuller, M.S., Sándor, G., Punske, B., Taccardi, B., MacLeod, R.S., Ershler, P.R., Green, L.S., and Lux, R.L. (2000a). Estimates of repolarization and its dispersion from electrocardiographic measurements: direct epicardial assessment in the canine heart. J. Electrocardiol. *33*, 171–180.

Fuller, M.S., Sándor, G., Punske, B., Taccardi, B., MacLeod, R.S., Ershler, P.R., Green, L.S., and Lux, R.L. (2000b). Estimates of repolarization dispersion from electrocardiographic measurements. Circulation *102*, 685–691.

Haws, C.W., and Lux, R.L. (1990). Correlation between in vivo transmembrane action potential durations and activation-recovery intervals from electrograms. Effects of interventions that alter repolarization time. Circulation *81*, 281–288.

Hockemeyer, D., Soldner, F., Cook, E.G., Gao, Q., Mitalipova, M., and Jaenisch, R. (2008). A drug-inducible system for direct reprogramming of human somatic cells to pluripotency. Cell Stem Cell *3*, 346–353.

Itzhaki, I., Maizels, L., Huber, I., Zwi-Dantsis, L., Caspi, O., Winterstern, A., Feldman, O., Gepstein, A., Arbel, G., Hammerman, H., et al. (2011). Modelling the long QT syndrome with induced pluripotent stem cells. Nature *471*, 225–229.

Itzhaki, I., Maizels, L., Huber, I., Gepstein, A., Arbel, G., Caspi, O., Miller, L., Belhassen, B., Nof, E., Glikson, M., and Gepstein, L. (2012). Modeling of catecholaminergic polymorphic ventricular tachycardia with patient-specific human-induced pluripotent stem cells. J. Am. Coll. Cardiol. *60*, 990–1000.

Ivashchenko, C.Y., Pipes, G.C., Lozinskaya, I.M., Lin, Z., Xiaoping, X., Needle, S., Grygielko, E.T., Hu, E., Toomey, J.R., Lepore, J.J., and Willette, R.N. (2013). Human-induced pluripotent stem cell-derived cardiomyocytes exhibit temporal changes in phenotype. Am. J. Physiol. Heart Circ. Physiol. *305*, H913–H922.

Kato, R., Venkatesh, N., Kamiya, K., Yabek, S., Kannan, R., and Singh, B.N. (1988). Electrophysiologic effects of desethylamiodarone, an active metabolite of amiodarone: comparison with amiodarone during chronic administration in rabbits. Am. Heart J. *115*, 351–359.

Ke, L., Meijering, R.A., Hoogstra-Berends, F., Mackovicova, K., Vos, M.J., Van Gelder, I.C., Henning, R.H., Kampinga, H.H., and Brundel, B.J. (2011). HSPB1, HSPB6, HSPB7 and HSPB8 protect against RhoA GTPase-induced remodeling in tachypaced atrial myocytes. PLoS ONE *6*, e20395.

Kodama, I., Kamiya, K., Honjo, H., and Toyama, J. (1996). Acute and chronic effects of amiodarone on mammalian ventricular cells. Jpn. Heart J. *37*, 719–730.

Kodama, I., Kamiya, K., and Toyama, J. (1997). Cellular electropharmacology of amiodarone. Cardiovasc. Res. *35*, 13–29.

Lahti, A.L., Kujala, V.J., Chapman, H., Koivisto, A.P., Pekkanen-Mattila, M., Kerkelä, E., Hyttinen, J., Kontula, K., Swan, H., Conklin, B.R., et al. (2012). Model for long QT syndrome type 2 using human iPS cells demonstrates arrhythmogenic characteristics in cell culture. Dis. Model. Mech. *5*, 220–230.

Liang, P., Lan, F., Lee, A.S., Gong, T., Sanchez-Freire, V., Wang, Y., Diecke, S., Sallam, K., Knowles, J.W., Wang, P.J., et al. (2013). Drug screening using a library of human induced pluripotent stem cell-derived cardiomyocytes reveals disease-specific patterns of cardiotoxicity. Circulation *127*, 1677–1691.

Lowry, W.E., Richter, L., Yachechko, R., Pyle, A.D., Tchieu, J., Sridharan, R., Clark, A.T., and Plath, K. (2008). Generation of human

induced pluripotent stem cells from dermal fibroblasts. Proc. Natl. Acad. Sci. USA *105*, 2883–2888.

Mace, L.C., Yermalitskaya, L.V., Yi, Y., Yang, Z., Morgan, A.M., and Murray, K.T. (2009). Transcriptional remodeling of rapidly stimulated HL-1 atrial myocytes exhibits concordance with human atrial fibrillation. J. Mol. Cell. Cardiol. *47*, 485–492.

Malan, D., Friedrichs, S., Fleischmann, B.K., and Sasse, P. (2011). Cardiomyocytes obtained from induced pluripotent stem cells with long-QT syndrome 3 recapitulate typical disease-specific features in vitro. Circ. Res. *109*, 841–847.

Matsa, E., Rajamohan, D., Dick, E., Young, L., Mellor, I., Staniforth, A., and Denning, C. (2011). Drug evaluation in cardiomyocytes derived from human induced pluripotent stem cells carrying a long QT syndrome type 2 mutation. Eur. Heart J. *32*, 952–962.

Moretti, A., Bellin, M., Welling, A., Jung, C.B., Lam, J.T., Bott-Flügel, L., Dorn, T., Goedel, A., Höhnke, C., Hofmann, F., et al. (2010). Patient-specific induced pluripotent stem-cell models for long-QT syndrome. N. Engl. J. Med. *363*, 1397–1409.

Navarrete, E.G., Liang, P., Lan, F., Sanchez-Freire, V., Simmons, C., Gong, T., Sharma, A., Burridge, P.W., Patlolla, B., Lee, A.S., et al. (2013). Screening drug-induced arrhythmia events using human induced pluripotent stem cell-derived cardiomyocytes and low-impedance microelectrode arrays. Circulation *128* (*Suppl 1*), S3–S13.

Nosten, F., ter Kuile, F.O., Luxemburger, C., Woodrow, C., Kyle, D.E., Chongsuphajaisiddhi, T., and White, N.J. (1993). Cardiac effects of antimalarial treatment with halofantrine. Lancet *341*, 1054–1056.

Qi, X.Y., Yeh, Y.H., Xiao, L., Burstein, B., Maguy, A., Chartier, D., Villeneuve, L.R., Brundel, B.J., Dobrev, D., and Nattel, S. (2008). Cellular signaling underlying atrial tachycardia remodeling of L-type calcium current. Circ. Res. *103*, 845–854.

Shiroshita-Takeshita, A., Brundel, B.J., and Nattel, S. (2005). Atrial fibrillation: basic mechanisms, remodeling and triggers. J. Interv. Card. Electrophysiol. *13*, 181–193.

So, E.C., Sallin, M.A., Zhang, X., Chan, S.L., Sahni, L., Schulze, D.H., Davila, E., Strome, S.E., and Jain, A. (2013). A high throughput method for enrichment of natural killer cells and lymphocytes and assessment of in vitro cytotoxicity. J. Immunol. Methods *394*, 40–48.

Sommer, C.A., Sommer, A.G., Longmire, T.A., Christodoulou, C., Thomas, D.D., Gostissa, M., Alt, F.W., Murphy, G.J., Kotton, D.N., and Mostoslavsky, G. (2010). Excision of reprogramming transgenes improves the differentiation potential of ips cells generated with a single excisable vector. Stem Cells *28*, 64–74.

Sommer, A.G., Rozelle, S.S., Sullivan, S., Mills, J.A., Park, S.M., Smith, B.W., Iyer, A.M., French, D.L., Kotton, D.N., Gadue, P., et al. (2012). Generation of human induced pluripotent stem cells from peripheral blood using the STEMCCA lentiviral vector. J. Vis. Exp. *68*, 4327.

Spitzer, K.W., Sato, N., Tanaka, H., Firek, L., Zaniboni, M., and Giles, W.R. (1997). Electrotonic modulation of electrical activity in rabbit atrioventricular node myocytes. Am. J. Physiol. *273*, H767–H776.

Staerk, J., Dawlaty, M.M., Gao, Q., Maetzel, D., Hanna, J., Sommer, C.A., Mostoslavsky, G., and Jaenisch, R. (2010). Reprogramming of human peripheral blood cells to induced pluripotent stem cells. Cell Stem Cell *7*, 20–24.

Takahashi, K., and Yamanaka, S. (2006). Induction of pluripotent stem cells from mouse embryonic and adult fibroblast cultures by defined factors. Cell *126*, 663–676.

Takahashi, K., Tanabe, K., Ohnuki, M., Narita, M., Ichisaka, T., Tomoda, K., and Yamanaka, S. (2007). Induction of pluripotent stem cells from adult human fibroblasts by defined factors. Cell *131*, 861–872.

Vaseghi, M., Yamakawa, K., Sinha, A., So, E.L., Zhou, W., Ajijola, O.A., Lux, R.L., Laks, M., Shivkumar, K., and Mahajan, A. (2013). Modulation of regional dispersion of repolarization and T-peak to T-end interval by the right and left stellate ganglia. Am. J. Physiol. Heart Circ. Physiol. *305*, H1020–H1030.

Yang, Z., Shen, W., Rottman, J.N., Wikswo, J.P., and Murray, K.T. (2005). Rapid stimulation causes electrical remodeling in cultured atrial myocytes. J. Mol. Cell. Cardiol. *38*, 299–308.

Yazawa, M., Hsueh, B., Jia, X., Pasca, A.M., Bernstein, J.A., Hallmayer, J., and Dolmetsch, R.E. (2011). Using induced pluripotent stem cells to investigate cardiac phenotypes in Timothy syndrome. Nature *471*, 230–234.

Yu, J., Vodyanik, M.A., Smuga-Otto, K., Antosiewicz-Bourget, J., Frane, J.L., Tian, S., Nie, J., Jonsdottir, G.A., Ruotti, V., Stewart, R., et al. (2007). Induced pluripotent stem cell lines derived from human somatic cells. Science *318*, 1917–1920.

Yue, A.M., Paisey, J.R., Robinson, S., Betts, T.R., Roberts, P.R., and Morgan, J.M. (2004). Determination of human ventricular repolarization by noncontact mapping: validation with monophasic action potential recordings. Circulation *110*, 1343–1350.

Zhang, Q., Jiang, J., Han, P., Yuan, Q., Zhang, J., Zhang, X., Xu, Y., Cao, H., Meng, Q., Chen, L., et al. (2011). Direct differentiation of atrial and ventricular myocytes from human embryonic stem cells by alternating retinoid signals. Cell Res. *21*, 579–587.

Zhang, J., Klos, M., Wilson, G.F., Herman, A.M., Lian, X., Raval, K.K., Barron, M.R., Hou, L., Soerens, A.G., Yu, J., et al. (2012). Extracellular matrix promotes highly efficient cardiac differentiation of human pluripotent stem cells: the matrix sandwich method. Circ. Res. *111*, 1125–1136.

Zhu, W.Z., Van Biber, B., and Laflamme, M.A. (2011). Methods for the derivation and use of cardiomyocytes from human pluripotent stem cells. Methods Mol. Biol. *767*, 419–431.

Zwi, L., Caspi, O., Arbel, G., Huber, I., Gepstein, A., Park, I.H., and Gepstein, L. (2009). Cardiomyocyte differentiation of human induced pluripotent stem cells. Circulation *120*, 1513–1523.

Stem Cell Reports, Volume *3*

Supplemental Information

Functional and Pharmacological Analysis of Cardiomyocytes Differentiated from Human Peripheral Blood Mononuclear-Derived Pluripotent Stem Cells

Michael Riedel, Chuanchau J. Jou, Shuping Lai, Robert L. Lux, Alonso P. Moreno, Kenneth W. Spitzer, Elizabeth Christians, Martin Tristani-Firouzi, and Ivor J. Benjamin

Supplemental Data

Supplemental Figures

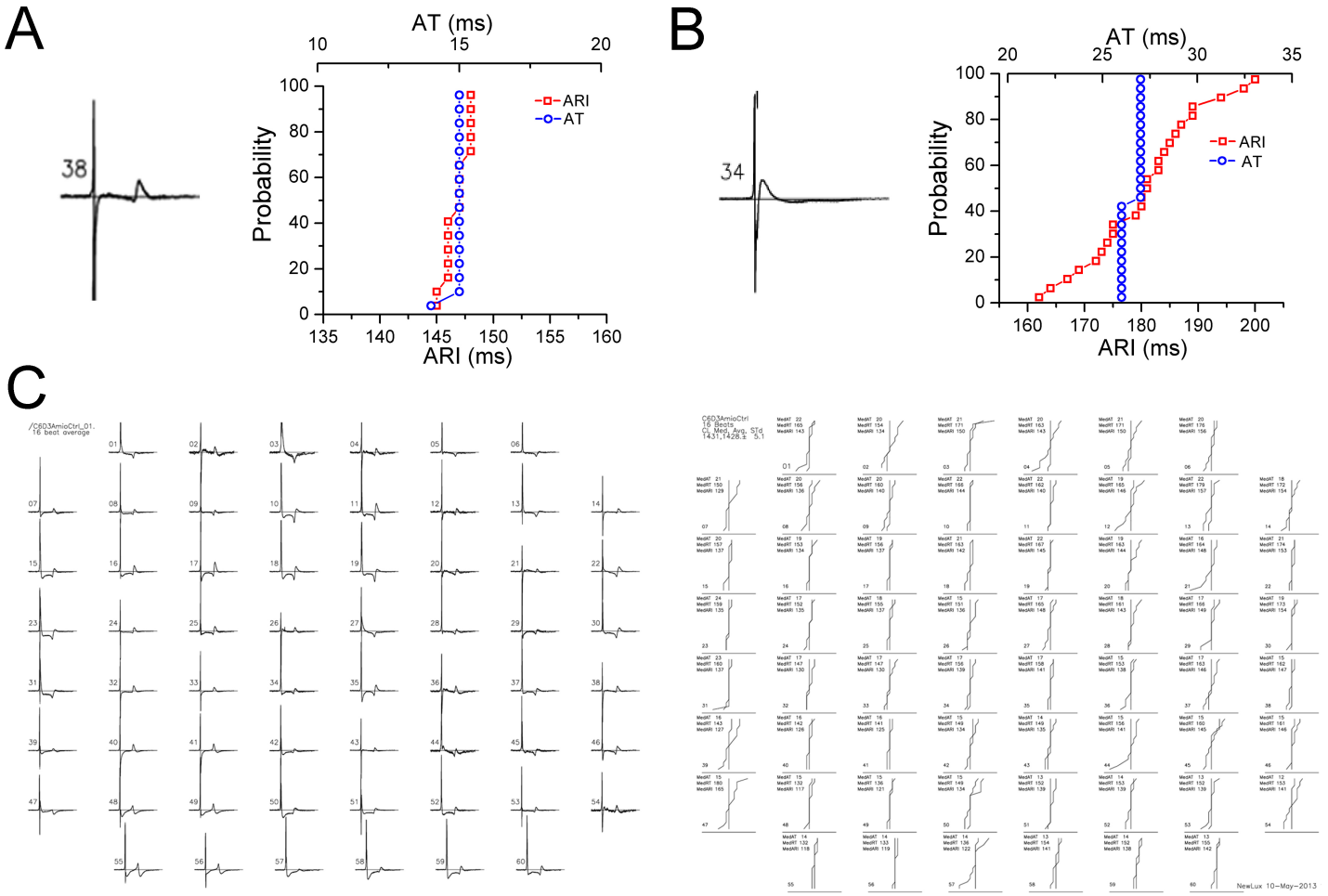

Figure S1. Methodology to assess the quality of MEA recordings, related to Figure 5.

Plots of the cumulative probability distribution functions (CPDFs) of activation times (AT) and activation-recovery intervals (ARI) for an electrogram displaying a well-defined T upstroke (**A**) and an electrogram with low amplitude repolarization waveform (**B**). Each plot shows all N measurements for each variable. The plots provide a means to reject outliers and thereby calculate average values while excluding 20% of the measurements at the extremes. **C**, Left panel shows the 60 individual MEA electrograms for a recording having excellent repolarization waveforms. The right panel shows all the CPDFs for ATs and ARIs from each electrogram. These measures were used to quality control the analyzed data and thereby improve precision.

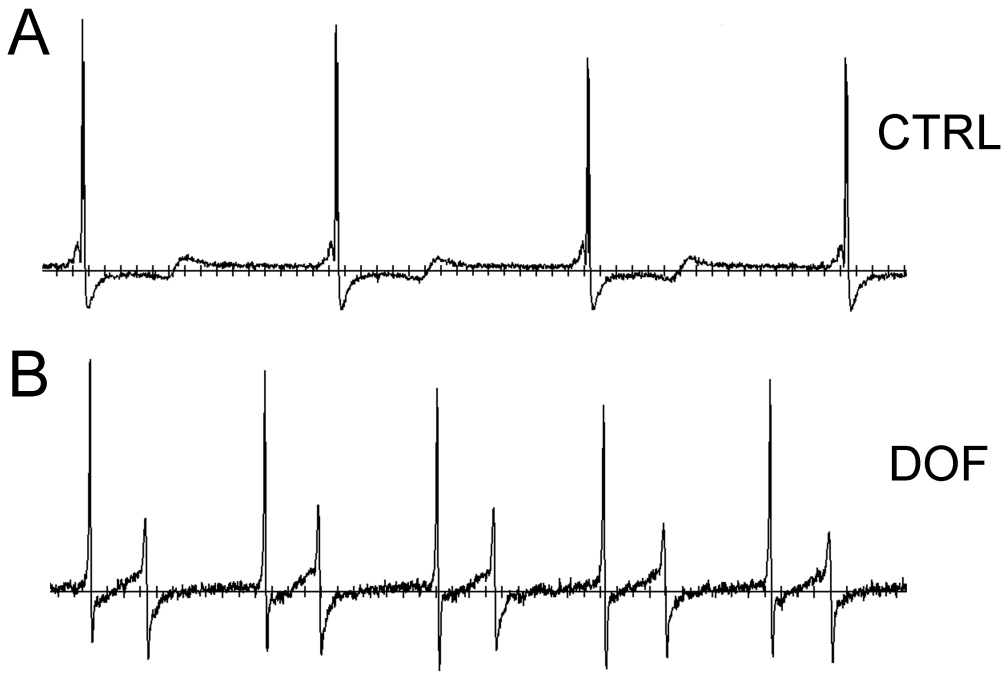

Figure S2. Early after-depolarizations induced by dofetilide, related to Figure 6. A, Baseline recording of local electrogram from the 60 MEA chamber in control solution. B, Same electrogram after perfusion with 10 nM dofetilide showing spontaneous depolarizations that emanate from repolarization time period. Each horizontal tick represents 50 ms. CTRL, control; DOF, dofetilide.

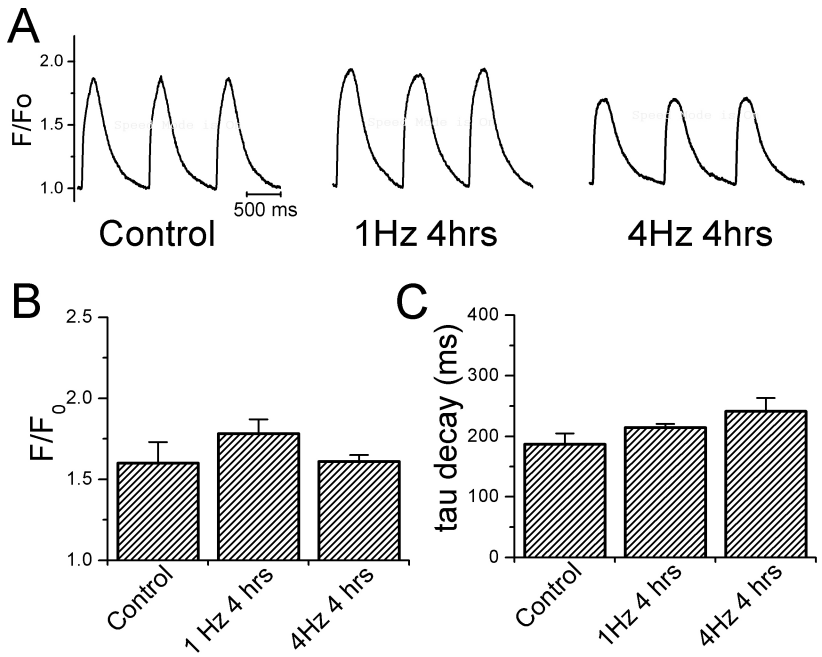

Figure S3. Rapid electrical stimulation for short periods of time (4 hrs) does not reduce Ca^{2+} transients, Related to Figure 7.

A, Representative Ca^{2+} transients recorded using fluo-4 labeled human iPSC-CM unpaced (control) and paced at 1Hz or 4 Hz for 4 hours. **B**, Bar graphs showing magnitude of Ca^{2+} transient expressed as F/F_0 and rate of transient decay (tau, ms). N=10 independent recordings, each group. Unlike rapid electrical stimulation for 8 hours, stimulation at 4 Hz for 4 hours did not alter the magnitude or rate of Ca^{2+} decay.

Supplemental Tables

Table S1. RT-qPCR primers for pluripotency gene characterizations

Hs_RRN18S_1_SG QuantiTect Primer Assay (200) Cat. No./ID: QT00199367	human *18S rRNA*
Hs_SOX2_1_SG QuantiTect Primer Assay (200) Cat. No./ID: QT00237601	human *SOX2*
Hs_NANOG_2_SG QuantiTect Primer Assay (200) Cat. No./ID: QT01844808	human *NANOG*
Hs_PODXL_1_SG QuantiTect Primer Assay (200) Cat. No./ID: QT00005138	human *TRA-1-60*
Hs_POU5F1_1_SG QuantiTect Primer Assay (200) Cat. No./ID: QT00210840	human *OCT4*

Table S2 . RT-qPCR primers for in vitro 3 germ layer characterizations

Hs_RRN18S_1_SG QuantiTect Primer Assay (200) Cat. No./ID: QT00199367	human *18S rRNA*
Hs_AFP1_1_SG QuantiTect Primer Assay (200) Cat. No./ID: QT00085183	human *AFP1*
Hs_GATA4_1_SG QuantiTect Primer Assay (200) Cat. No./ID: QT00031997	human *GATA4*
Hs_MYH6_1_SG QuantiTect Primer Assay (200) Cat. No./ID: QT00030807	human cardiac *MYH6*
Hs_T_1_SG QuantiTect Primer Assay (200) Cat. No./ID: QT00062314	human *BRACHYURY*
Hs_TUBB3_1_SG QuantiTect Primer Assay (200) Cat. No./ID: QT0083713	human *β-III-TUBULIN*
Hs_VIM_1_SG QuantiTect Primer Assay (200) Cat. No./ID: QT00095795	human *VIMENTIN*

Table S3. Antibodies used in this study.

NANOG	abcam ab80892
SSEA4	abcam ab16287
OCT4	abcam ab27985
TRA-1-81	abcam ab16289
cardiac TROPONIN T	abcam ab45932
sarcomeric α-ACTININ	Sigma A7732

Supplemental Methods

Measurement of intracellular calcium

Calcium transients (CaTs) were detected in human iPSC-CMs with an epifluorescence system using the fluorescent indicator fluo-4 AM (Molecular Probes). Cells were bathed in a buffered physiological solution containing 7.5 mM fluo-4 AM for 3 minutes, then transferred to a recording chamber coated with poly-l-Lysine and continuously perfused with a physiological solution 37^{o}C. CaTs were recorded from spontaneously beating cell clusters or clusters paced at various cycle lengths using an external field stimulator. Fluorescence emission (535 ± 11 nm, band-pass filter) was collected with a photomultiplier tube via the ×40 oil objective (numerical aperture 1.3) during continuous excitation at 485 nm with a 150-W Xenon lamp. Fluorescence signals were background corrected and expressed as F/F_0 (the ratio of fluorescence during the CaT divided by diastolic fluorescence). The time course of CaT decay (tau decay) was meaured by fitting the decay phase to a monoexponential function. All measurements were performed in triplicate.